The 2nd IBS Conference on Exotic Nuclei (ICEN2026) | July 24, 2026 | IBS Science Culture Center, Daejeon

Development of a Quadrant Silicon Pad Sensor for the TexAT Active Target Detector

Gyoung Mo Gu[1,2], Kyung Yuk Chae[1], Jong Won Hwang[2], Kevin Insik Hahn[2], Jin-A Jeon[3], Min-Bin Kim[3], Sunghoon Ahn[2] and **Hye Young Lee**[2]* (speaker)

[1] Department of Physics, Sungkyunkwan University
[2] Center for Exotic Nuclear Studies, Institute for Basic Science
[3] Center for Underground Physics, Institute for Basic Science

Published in *Sensors 2026, 26, 3147* · doi:10.3390/s26103147

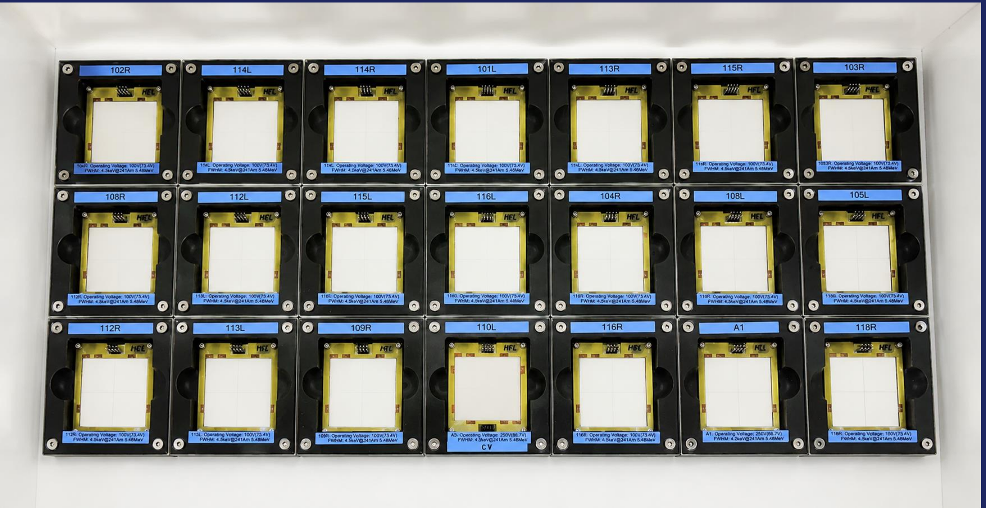

Motivation: Single Texas Active Target TPC (TexAT)

– TexAT enables a broad range of nuclear physics experiments with rare isotope beams — resonance scattering, transfer reactions, β-delayed decay — where **detector performance directly determines what physics is accessible.**

– TexAT combines a Micromegas-based TPC for 3D track reconstruction with a surrounding **Si + CsI(Tl) wall** for total energy measurement and PID.

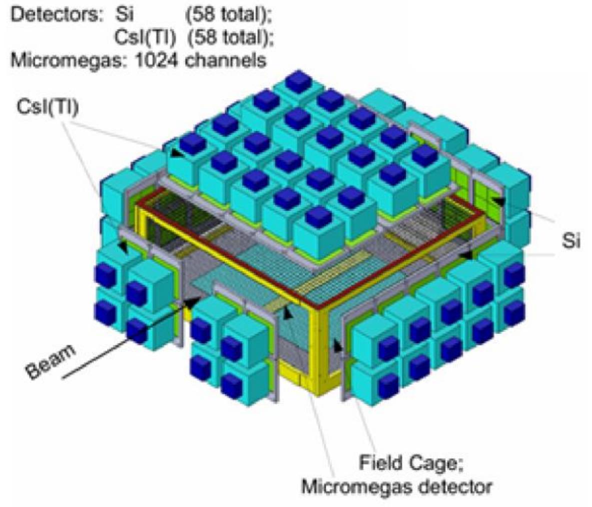

– **Solid-State Detector Array (Si + CsI(Tl))**

- High segmentation of the Si wall is not required, as 3D tracking is already performed in the TPC
- Single-sided quadrant silicon detectors with an active area of 50×50 mm² form the Si detector wall
- Key requirements: **high energy resolution + reliability + cost effectiveness**

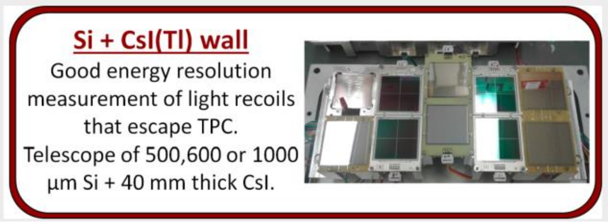

– **Korean Team's Contribution**

With the aim of securing a **stable detector supply and establishing independent fabrication capability** for participation in the TexAT experiment, a quadrant silicon pad sensor optimized for the TexAT geometric design was independently designed, fabricated, and delivered for use in the experiment.

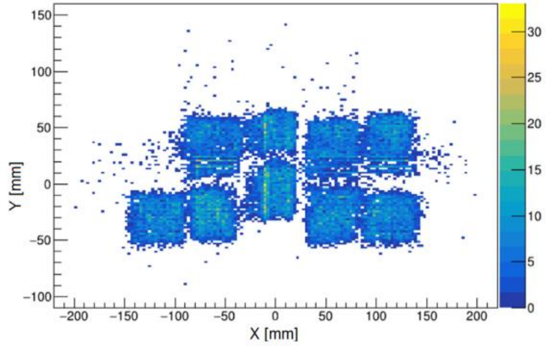

Fig. 23. The XZ projection of the forward Si wall.

Quadrant Silicon Pad Sensor Design & Fabrication

Wafer	6-inch n-type ⟨100⟩ silicon, >5 kΩ·cm, 550 μm thick
Structure	$p^+/n/n^+$ junction, p^+ depth < 1 μm
Active area	5 × 5 cm^2 total, 4 quadrants of 2.5 × 2.5 cm^2
Metallization	Al (thickness: 0.5 μm) (full-window: light-tight, no charge-up)
Process	~50 single-sided steps, 4 photolithography stages Fabricated at ETRI in Korea
Full depletion	≈ 150 V
Termination	G6 / G9 / G14 guard-ring variants fabricated

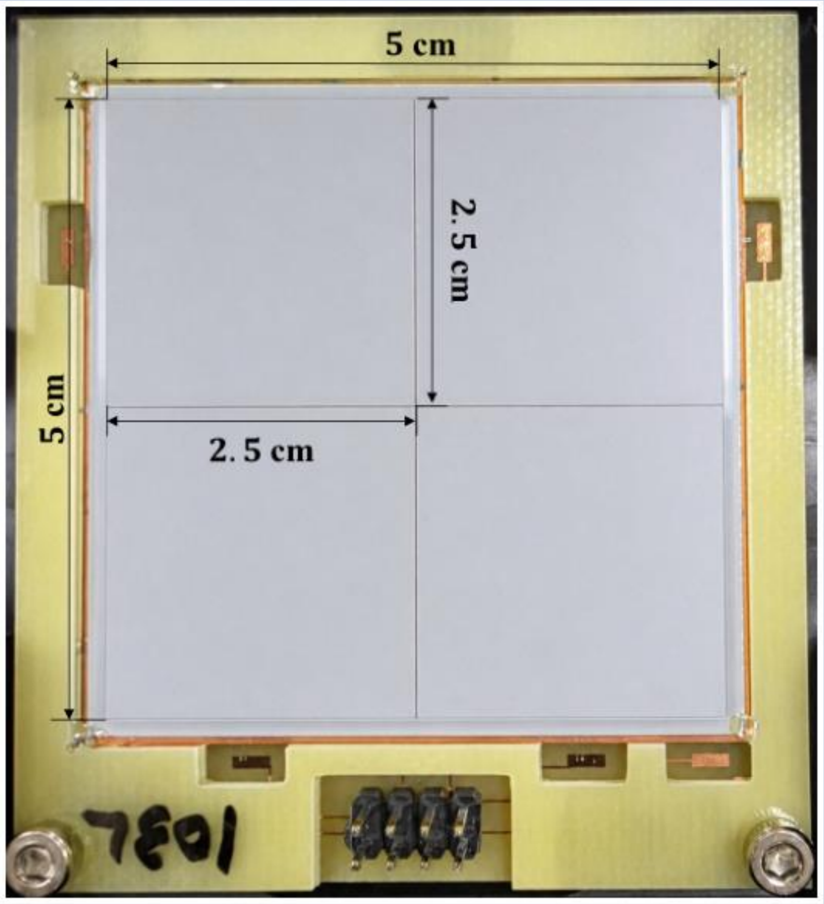

Fabricated quadrant sensor mounted on its PCB

ETRI Semiconductor Laboratory

Premature Breakdown at the Sensor Edge

(a)

(b)

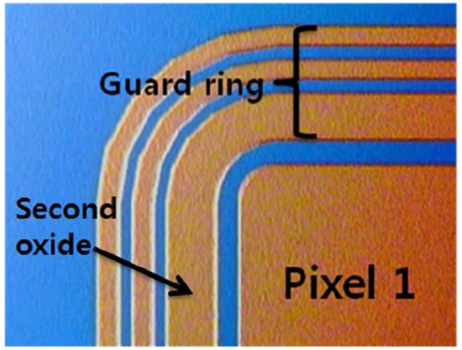

36ch-Pad Sensors with an active area of 6.2 x 6.2 cm^2 for the Electromagnetic Calorimeter of the Linear Collider Experiment

(a)

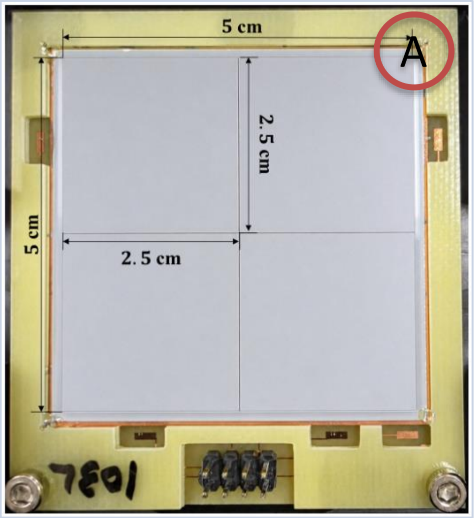

(b)

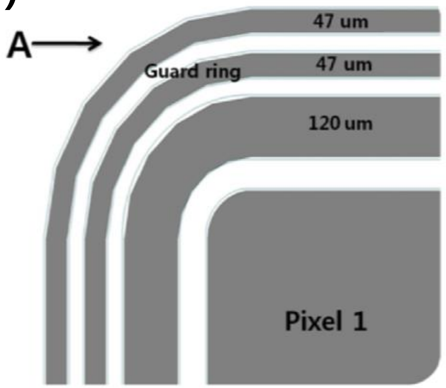

Fabricated quadrant sensor mounted on its PCB

Two cases showing different results when using the same guard ring design :

- In finely segmented sensors, the many inter-pad gaps spread the lateral E-field; only **3 guard-rings** were needed in our previous 36ch-pad sensors. The sensor had low leakage current without premature breakdown up to 200V
- In large 2.5 × 2.5 cm^2 segments, lateral E-field relaxation is limited and the E-field **concentrates at the device edge.** Therefore, premature breakdown is likely to occur.

When using 3 guard rings for the quadrant sensor, the first prototype broke down at about **40 V**, far below the required full-depletion voltage of about **150 V**.

▶ The guard-ring termination design is therefore critical for reaching full depletion

Guard-Ring Termination Designs: G6, G9, G14

Figure 1. Guard-ring layouts analyzed in this study: (**a**) 6 rings (G6), (**b**) 9 rings (G9), and (**c**) 14 rings (G14) configurations. The region labeled A denotes the active area, and 1st guard-ring(the innermost thick guard-ring) is identical in all designs. so the differences are only in the outer arrangement.

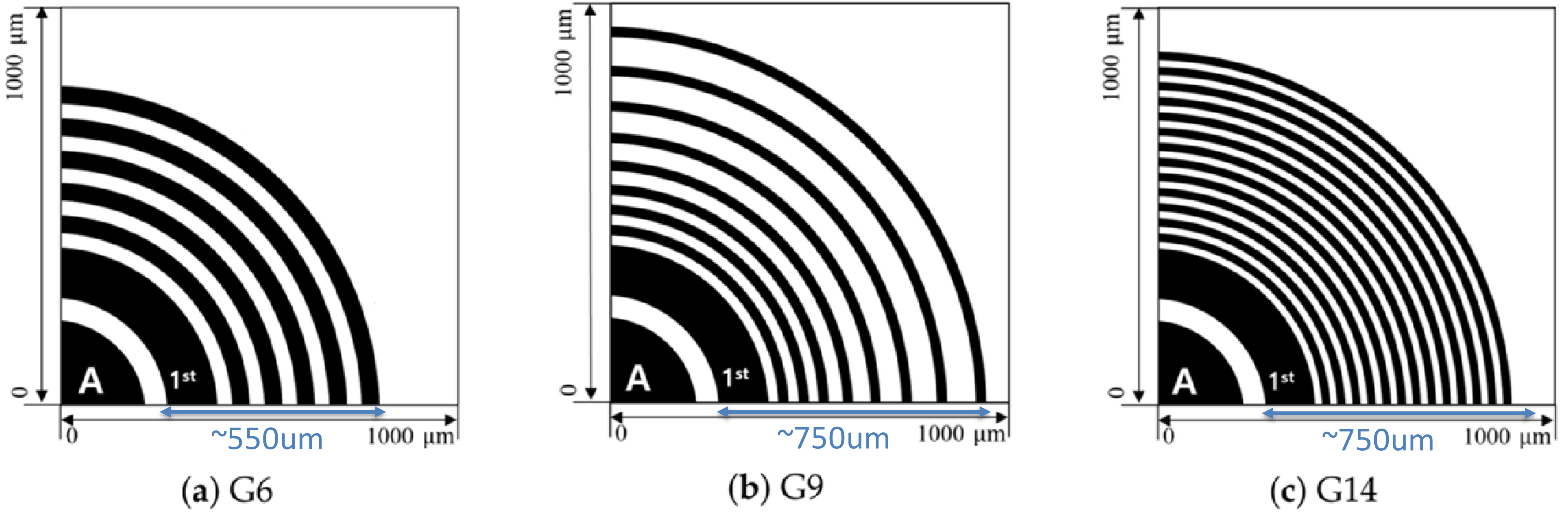

G6: initial design

Total termination width comparable to the wafer thickness (550 µm); uniform wide rings

G9: graded spacing

Dense rings near the active area, wider spacing toward the edge; narrower rings, wider termination

G14: uniform spacing

Same ring width as G9; equal spacing across the whole termination

(G9 and G14 share a similar termination area, both significantly wider than that of G6)

TCAD Simulation of the Termination Region

Device characteristics were analyzed using Technology Computer-Aided Design (TCAD) simulations implemented in Silvaco ATLAS.

To compare the designs we ran TCAD simulations with Silvaco, using doping profiles and process conditions consistent with the actual fabrication.

Figure 2. Two-dimensional electric-field distributions in the vertical cross-section for (**a**) G6, (**b**) G9, and (**c**) G14 structures.

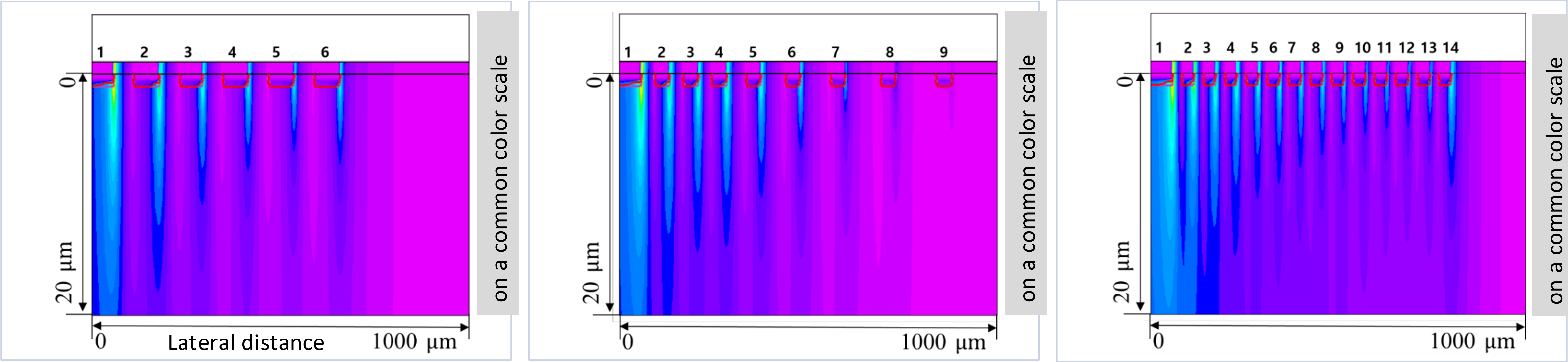

(a) G6 (b) G9 (c) G14

- Reverse bias is applied to the active electrode, the back side is grounded, and all guard rings are left floating, as they are operated in practice.
- E-Field distributions are similar near the active area; clear differences appear in the **outer termination region**

1D Electric-Field Profiles along the Termination

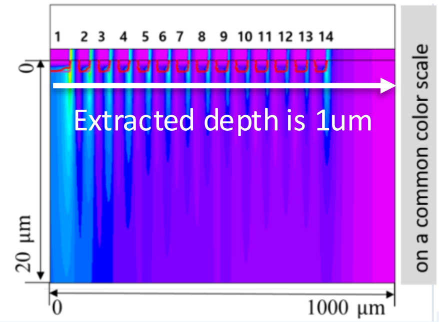

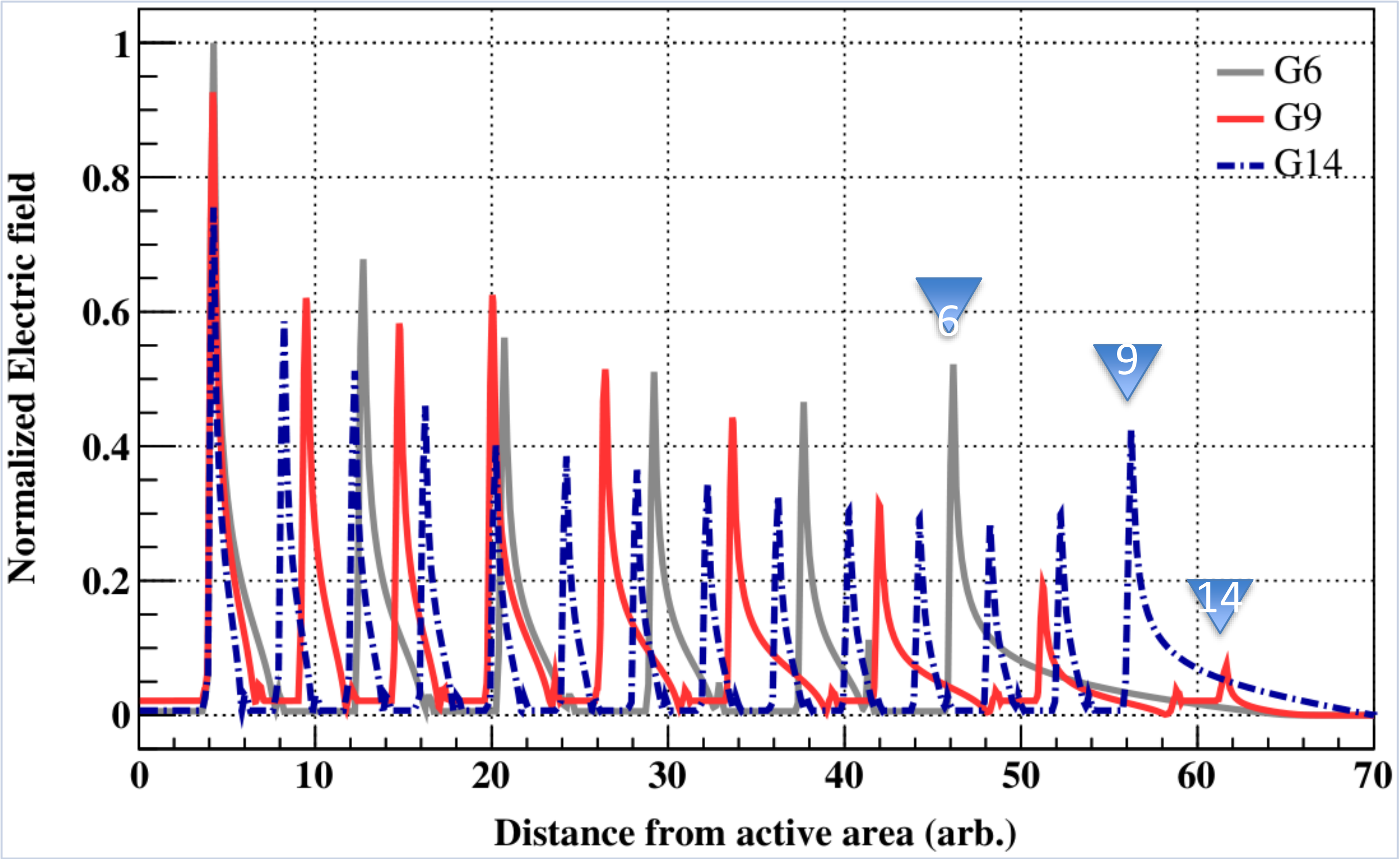

G6 E-Field remains high across the whole termination and rises again at the outermost ring (field crowding)

G14 E-field decreases stepwise, but crowding also remains at the last ring despite the larger number of rings and the wider termination

G9 Graded spacing relaxes the field to nearly zero at the edge; no crowding

2D slice model: a qualitative comparison of field relaxation, not a quantitative breakdown prediction

Figure 3. Comparison of 1D electric-field profiles for the three guard-ring designs. Each spike here is a guard ring, and the y-axis is the field magnitude normalized to the peak at the first ring. The magnitude of the electric field was extracted along the lateral direction at a specific junction depth from the 2D distributions shown in Figure 2.

1D Electric-Field Profiles along the Termination

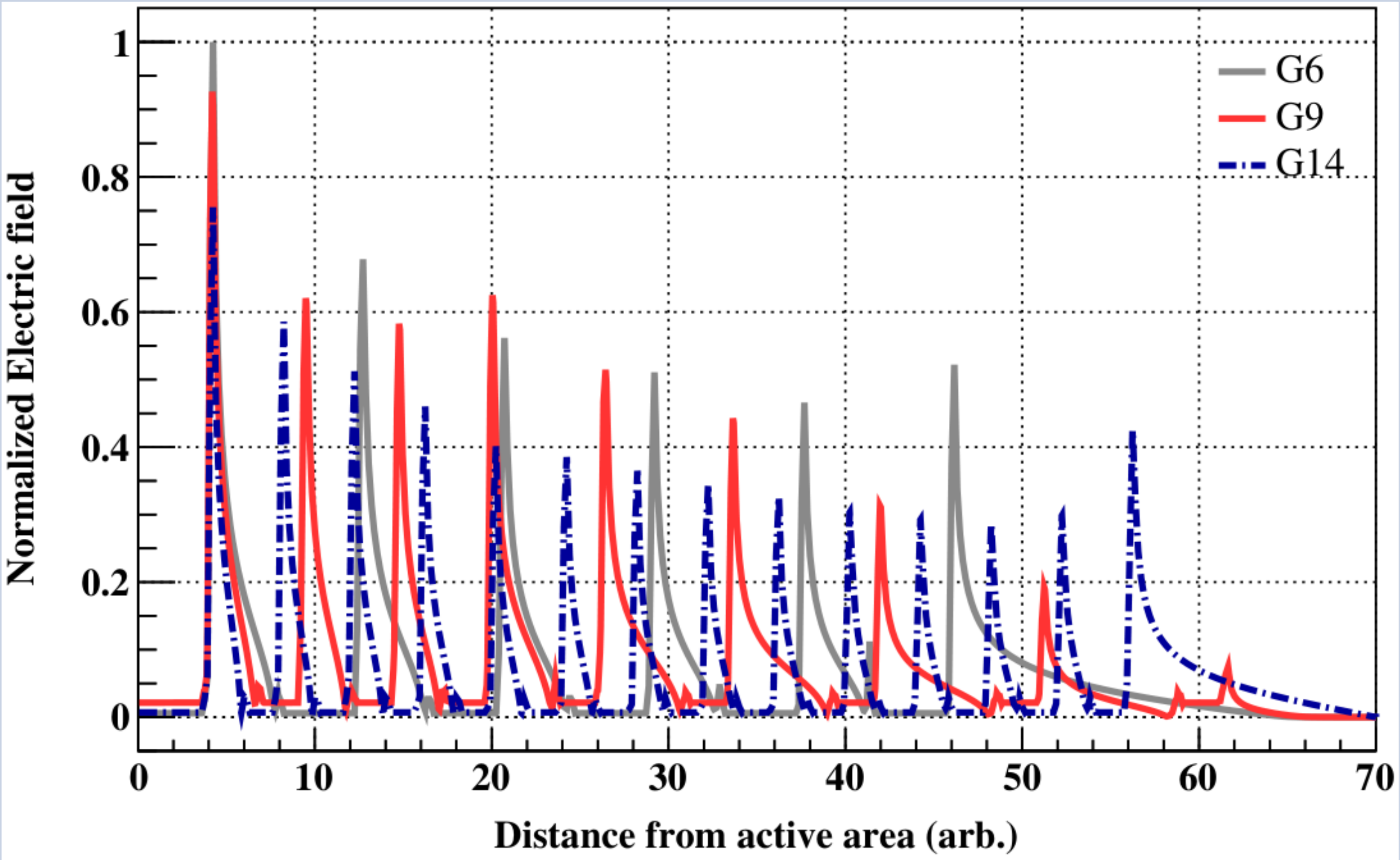

Summary

-These results show that **simply increasing the number of rings or widening the termination region is not enough** to ensure electrical stability.

-**What matters more is the strategic spacing between rings,** as demonstrated by G9.

Based on these findings, all three designs were fabricated and experimentally evaluated.

Figure 3. Comparison of 1D electric-field profiles for the three guard-ring designs. Each spike here is a guard ring, and the y-axis is the field magnitude normalized to the peak at the first ring. The magnitude of the electric field was extracted along the lateral direction at a specific junction depth from the 2D distributions shown in Figure 2.

CV Characteristics: Full Depletion at ~150 V

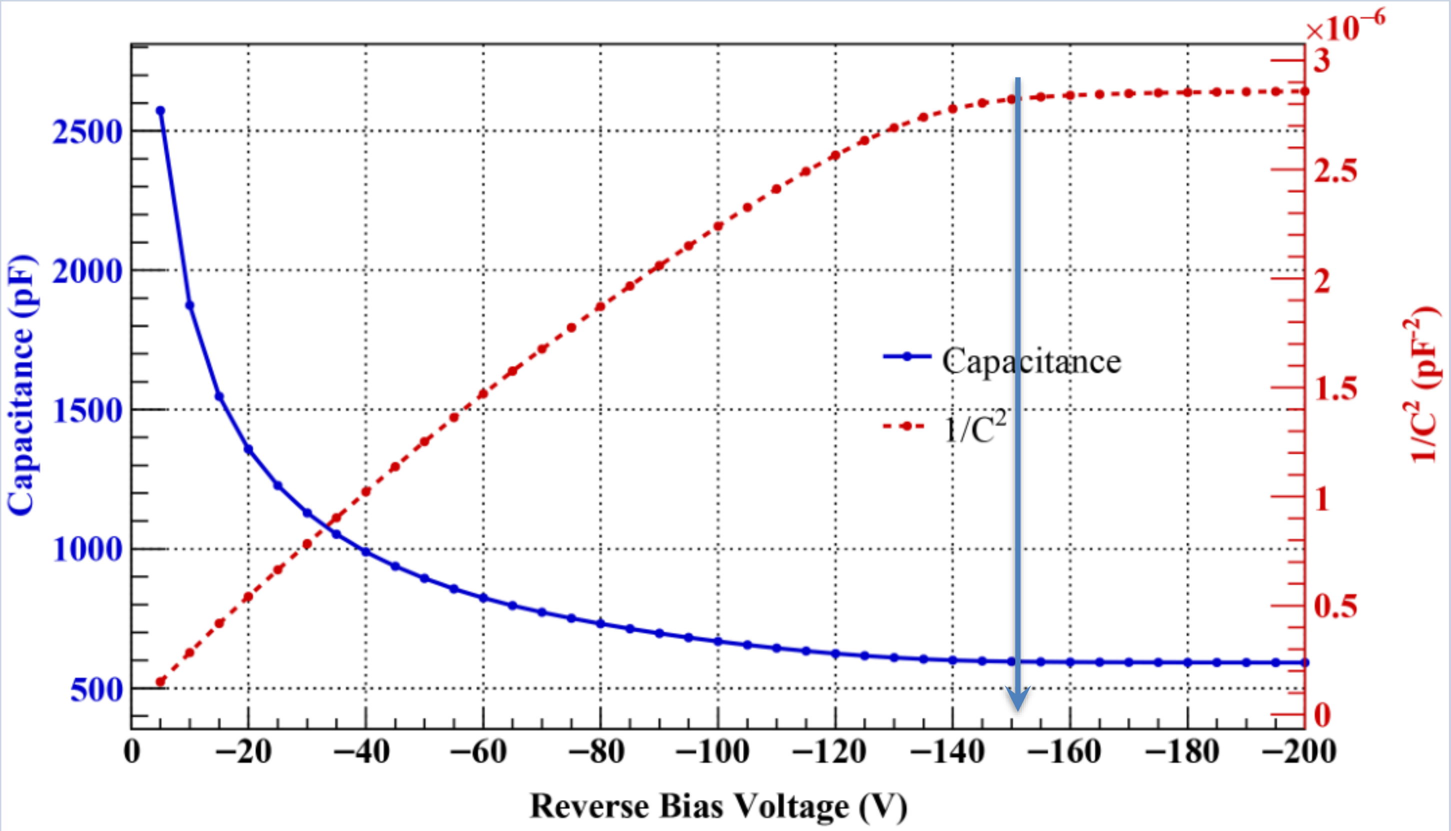

– CV measured at 1 MHz; IV with a picoammeter; the same reverse bias on all four pads, **guard-rings floating**

– Saturation of $1/C^2$ gives $\mathbf{V_{fd}}$ **≈ 140–150 V**, consistent with the substrate specifications

– IV range extended to −200 V to verify the operating margin beyond full depletion

Figure 4. Typical capacitance–voltage (CV) and 1/C2 characteristics of the fabricated sensor with a thickness of about 550 µm. The results were obtained from **the G9 structure**, which features a high bulk resistivity of over 5 kΩ·cm. The 1/C2 curve is used to determine the full depletion voltage by identifying the saturation point of the capacitance.

IV Characteristics: G9 and G14 Stable up to −200 V

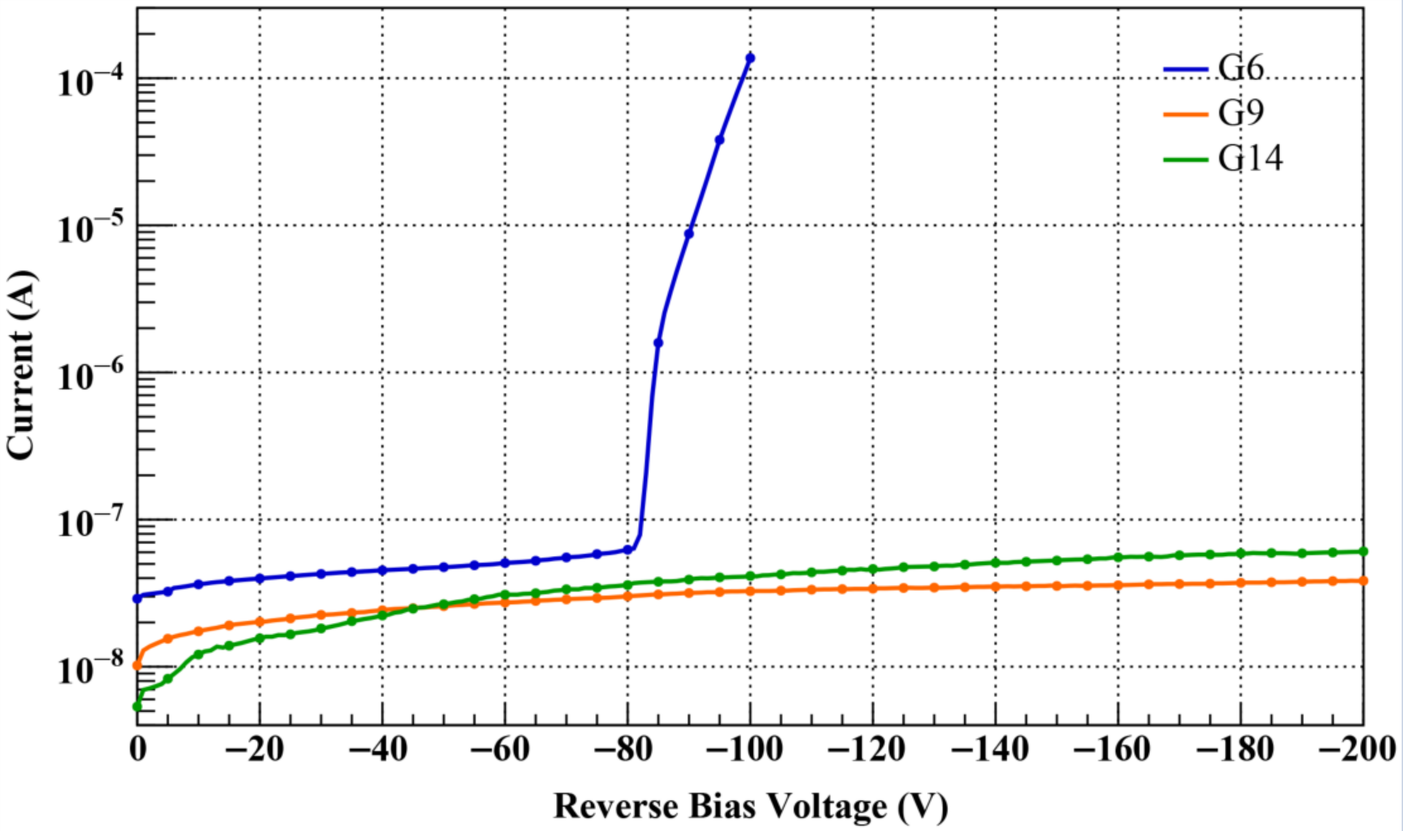

Figure 5. Comparison of current–voltage (IV) characteristics for sensors with G6, G9, and G14 guard-ring configurations. The results show that the premature breakdown observed in the G6 design around −80 V was effectively eliminated in the G9 and G14 designs. The sensors with optimized termination structures maintained stable leakage current at several tens of nA up to −200 V.

– **G6:** premature breakdown**,** rapid current increase from **−80 V**, reaching tens of μA at −100 V, consistent with the TCAD result

– **G9 and G14**: **stable up to −200 V** with leakage of **tens of nA**; no breakdown well beyond full depletion

– **G9 vs G14 (beyond −200 V):** Based on the simulation results, G9 is expected to offer more stable operation at higher reverse bias voltages than G14

G9 adopted as the final design

Best field relaxation in TCAD with fewer guard-rings

Energy Resolution with α Sources

α spectra: ^{148}Gd 3.18 MeV (left) and ^{241}Am 5.48 MeV (right), Gaussian fits in red

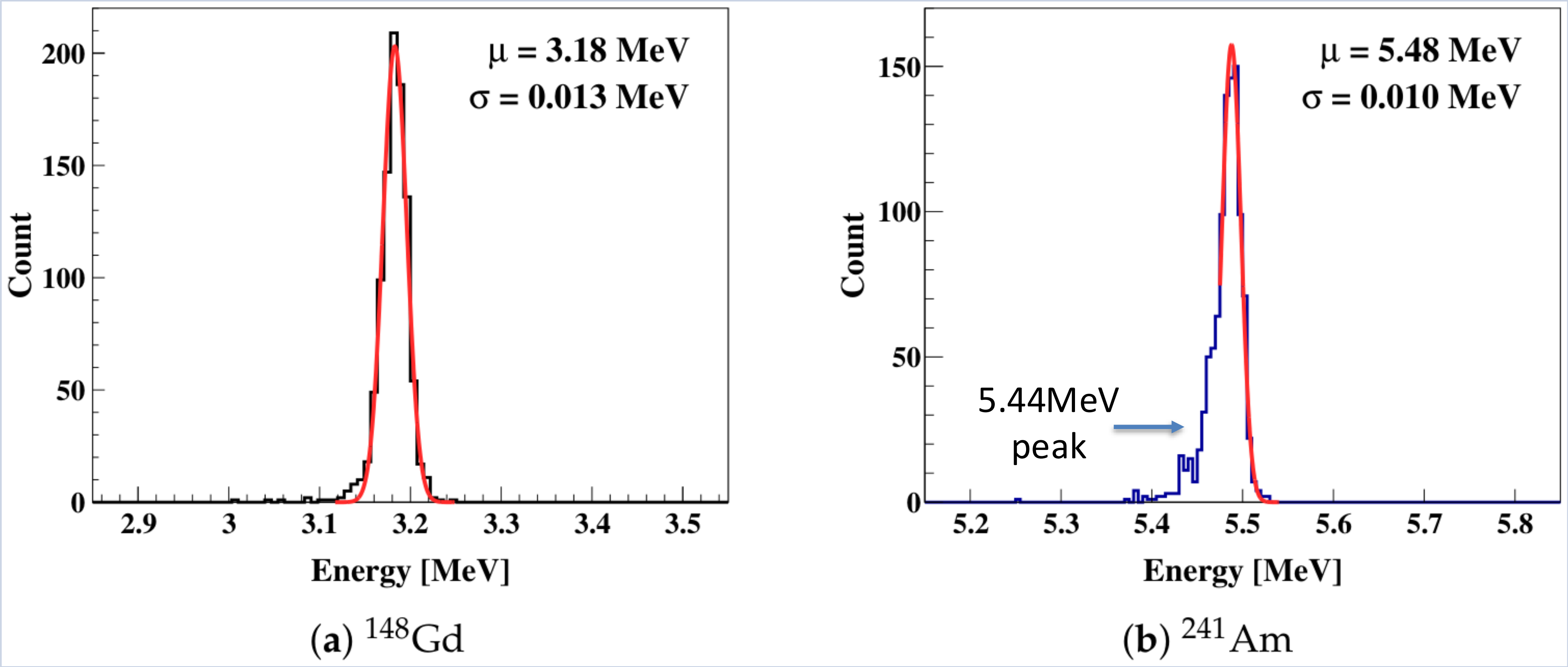

31 keV

FWHM at 3.18 MeV (^{148}Gd), ≈1% resolution

< 30 keV

FWHM at 5.48 MeV (^{241}Am), ≈0.54% resolution

- Stable signal formation and efficient charge collection despite the large-area pads

Sensor Production and Quality Assurance for TexAT

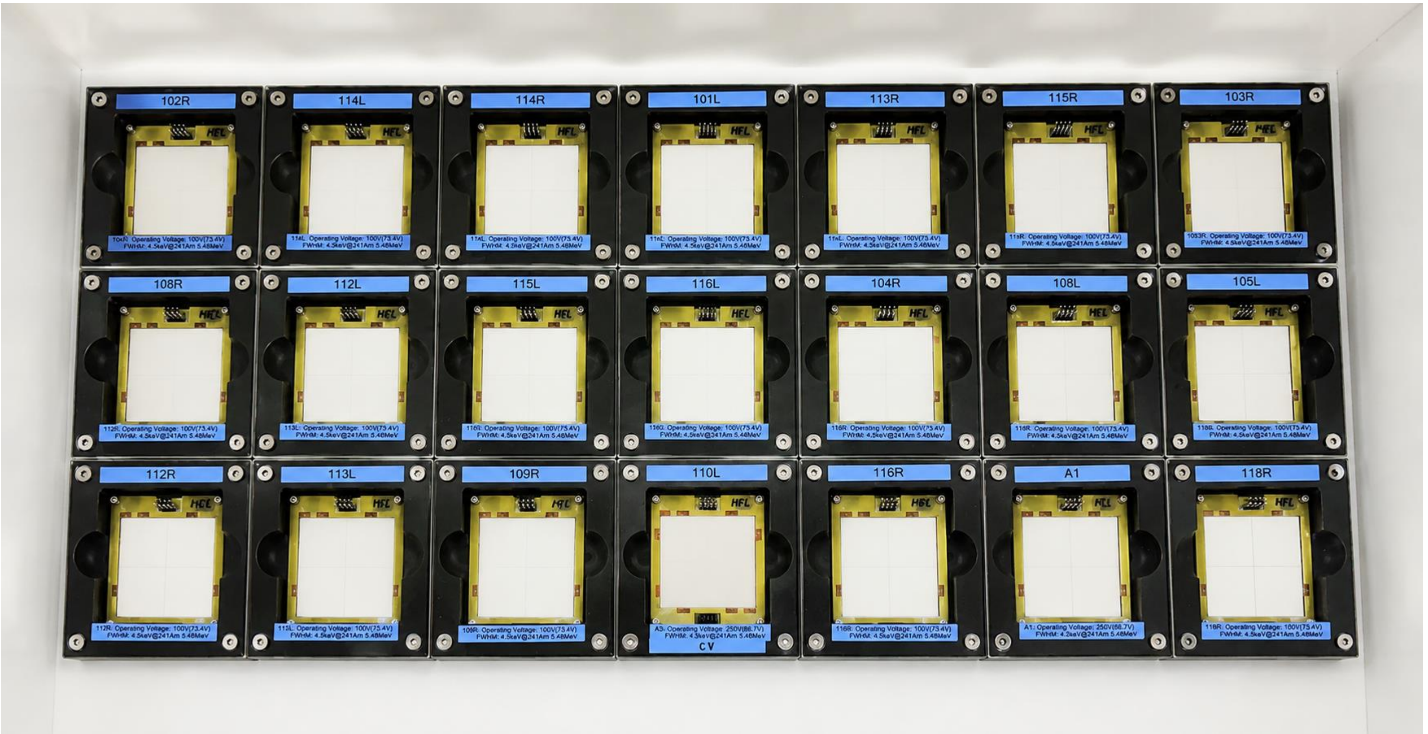

A total of 21 quadrant silicon pad sensors were successfully fabricated for the TexAT experiment.

- All 21 sensors underwent electrical characteristics testing and **laboratory-based radioactive source testing** (^{148}Gd, 3.18 MeV α) to verify energy resolution and leakage current performance
- Sensors confirmed to meet the required specifications for deployment in TexAT
- **Currently in preparation for shipping** to Texas A&M University
- All 21 sensors are scheduled to be **installed and used in the TexAT experiment**

Summary & Outlook

A 5 × 5 cm², four-channel quadrant silicon pad sensor was developed and validated for the TexAT detector

Design criterion	Stability of large-area segmented sensors is governed by the guard-ring spacing strategy rather than the number of rings: dense spacing near the active area, gradually wider toward the edge (G9)
Electrical	Premature breakdown eliminated; leakage current of tens of nA up to −200 V, well beyond full depletion (≈150 V)
Performance	31 keV FWHM (≈1%) for 3.18 MeV α particles, 30 keV FWHM (0.541%) for 5.48 MeV α particles
Production	A total of 21 quadrant silicon pad sensors with G9 design were successfully fabricated for the TexAT experiment. Currently in preparation for shipping to Texas A&M University.

Outlook: All 21 sensors are scheduled for installation in the TexAT experiment at Texas A&M — fulfilling our goal of securing a stable detector supply and establishing independent fabrication capability. These results also serve as useful design criteria for large-area silicon detectors in next-generation rare-isotope experiments.